Static dielectric response and Born effective charge of BN nanotubes from *ab initio* finite electric field calculations

G. Y. Guo,[1,2,*] S. Ishibashi,[1] T. Tamura,[1] and K. Terakura[3]
[1]*Research Institute for Computational Sciences (RICS), National Institute of Advanced Industrial Science and Technology (AIST), Tsukuba, Ibaraki 305-8568, Japan*
[2]*Department of Physics and Center for Theoretical Sciences, National Taiwan University, Taipei 10617, Taiwan*
[3]*Creative Research Institute "Sousei," Hokkaido University, Sapporo 001-0021, Japan*
(Received 12 February 2007; revised manuscript received 30 March 2007; published 5 June 2007)

Ab initio investigations of the full static dielectric response and Born effective charge of BN nanotubes (BN-NTs) have been performed using finite electric-field method. It is found that the ionic contribution to the static dielectric response of BN-NTs is substantial and also that a pronounced chirality-dependent oscillation is superimposed on the otherwise linear relation between the longitudinal electric polarizability and the tube diameter (D), as for a thin dielectric cylindrical shell. In contrast, the transverse dielectric response of the BN-NTs resembles the behavior of a thin (nonideal) conducting cylindrical shell of a diameter of $D+4$ Å, with a screening factor of 2 for the inner electric field. The medium principal component Z_y^* of the Born effective charge, corresponding to the transverse atomic displacement tangential to the BN-NT surface, has a pronounced D dependence (but independent of chirality), while the large longitudinal component Z_z^* exhibits a clear chirality dependence (but nearly D independent), suggesting a powerful way to characterize the diameter and chirality of a BN-NT.

DOI: 10.1103/PhysRevB.75.245403 PACS number(s): 73.63.Fg, 77.22.−d, 78.67.Ch

I. INTRODUCTION

Since the discovery of carbon nanotubes (CNTs) in 1991,[1] carbon and other nanotubes have attracted considerable interest worldwide because of their unusual properties and great potentials for technological applications. For example, semiconducting CNTs could function as nanoscale field-effect transistors.[2] It was also predicted that nanotori formed from metallic CNTs may exhibit giant paramagnetic moments.[3] Though CNTs continue to attract great interest, other nanotubes such as BN nanotubes[4] (BN-NTs) are interesting in their own right and may offer different possibilities for technological applications that CNTs cannot provide. In particular, as far as the optical and optoelectronic applications of nanotubes are concerned, BN-NTs could be superior to CNTs because BN-NTs are uniformly insulating, independent of their chirality.[5] Furthermore, recent experiments indicate that BN-NTs exhibit stronger resistance to oxidation at higher temperatures than CNTs.[6]

Therefore, the properties of both single-walled and multi-walled BN-NTs have been intensively studied experimentally and theoretically in recent years. In this paper, we focus on the dielectric response, including static dielectric constant, electric polarizability, and Born effective charge, of BN-NTs. A detailed knowledge of dielectric response is needed, e.g., to characterize optical excitations, screening at contacts, and plasmons in nanotube arrays. Variations in size and chirality may or may not affect dielectric properties, which in turn may be exploited to align nanotubes during, e.g., plasma-enhanced chemical-vapor deposition synthesis,[7,8] and to separate different tubes in solutions.[9] Synthesis and separation of specific nanotubes remain an important challenge.

Previously, the static electric polarizability for BN-NTs of a finite length has been calculated within a semiempirical dipole-dipole interaction model (up to 30 Å long) and also at the self-consistent field level (up to 20 Å long).[10] The static dielectric constant and electric polarizability of long nanotubes were typically obtained as the zero-frequency limit of the optical conductivity (see, e.g., Refs. 11 and 12 and references therein), which is calculated using either semiempiral tight-binding method or *ab initio* local-density approximation (LDA) or generalized gradient approximation within independent particle linear-response theory (IPLRT). In this way, only the electronic contribution to the static dielectric constant (ϵ_∞) is calculated.[11–14] Furthermore, local field effects, which can be substantial for the electric field applied perpendicular to the tube axis,[13] are neglected.[11,12] Here, we apply the latest finite-field electric-enthalpy theory[15,16] to study the static dielectric properties of BN-NTs. This theory allows us not only to obtain the full dielectric constants including both electronic and ionic contributions but also to include the local field effects. Furthermore, also using this theory, we perform the systematic study of the Born effective charge of the BN-NTs. A knowledge of the dependence of Born effective charge on the diameter and chirality of the nanotubes not only is important to understand their dynamical properties but also would allow us to characterize the nanotubes using, e.g., Raman and infrared spectroscopies.

II. THEORY AND COMPUTATIONAL DETAILS

We use the latest finite-field electric-enthalpy theory[15,16] to calculate field-induced electric polarization **P** and atomic forces **F**. For a small finite field **E**, the dielectric constant is $\epsilon_{\alpha\beta}=\delta_{\alpha\beta}+4\pi\chi_{\alpha\beta}$, where $\chi_{\alpha\beta}=P_\alpha/E_\beta$. If the atoms are kept fixed, this yields the electronic contribution ϵ_∞ (so-called clamped-ion dielectric constant), and if both the electrons and atoms are allowed to relax in response to the field, the full static dielectric constant ϵ_{static} is obtained. The electric polarizability α is given by $\epsilon_{\alpha\beta}=\delta_{\alpha\beta}+4\pi\alpha_{\alpha\beta}/\Omega$, where Ω is

the unit cell volume. The Born effective charge on the jth atom is $e\mathbf{Z}^*_{j\alpha\beta}=F_{j\beta}/E_\alpha$. Traditionally, the Born effective charge is obtained via $e\mathbf{Z}^*_{j\alpha\beta}=\Omega(\partial P_\alpha/\partial u_{j\beta})|_{\mathbf{E}=0}$, where u_j is the displacement of the jth atom due to the optical phonon mode, and is usually calculated by the finite difference approach. Therefore, the finite-field calculations have an advantage of being simple and less CPU-time consuming especially for complex systems such as BN-NTs.

We consider a number of representative BN-NTs with a range of diameters from all three types of BN-NTs, namely, the zigzag $[(n,0)$, $n=5,6,8,10,12,16]$, armchair $[(n,n)$, $n=3,4,6,8,12]$, and chiral (4,2), (5,2) BN-NTs. For comparison, we also study the dielectric properties of bulk BN in the cubic, wurtzite, and hexagonal structures (denoted as c-BN, w-BN, and h-BN, respectively), as well as a single honeycomb BN sheet. Our *ab initio* calculations were performed using accurate projector augmented-wave method,[17] as implemented in the Quantum Materials Simulator (QMAS) package.[18] A supercell geometry was adopted so that the nanotubes are aligned in a square array with the closest interwall distance between adjacent nanotubes being 9 Å. The isolated BN sheet is simulated by a slab-supercell approach with an intersheet distance of 15 Å. A plane-wave cutoff of 35 Ry was used throughout. For BN-NTs, a $2\times2\times n$ mesh in the first Brillouin zone is used throughout. For the achiral nanotubes, $n=8$, and for the chiral nanotubes, $n=6$. The ideal nanotubes were first constructed by rolling-up a honeycomb BN sheet. Their atomic positions and lattice constants were then fully relaxed until all the atomic forces and the stress were less than 4.0×10^{-5} and 1.0×10^{-6} Ry/bohr,[3] respectively. The same force and stress convergence criteria were used in the finite field calculations. The small finite field used is 0.001 a.u.[16] The calculated field-induced polarization and Born effective charge for the field perpendicular to the tube axis were checked with the usual sawtooth potential method, which cannot be applied for the field parallel to the tube axis, and the results from both approaches agree with each other very well (up to the third digit). Note that the unit cell volume Ω is not well defined for nanotubes and the single BN sheet. Therefore, like the previous calculations,[11,12] we used an effective unit cell volume of the nanotubes and the BN sheet rather than the volume of the supercells which is arbitrary. The effective unit cell volume for a nanotube and the BN sheet is given, respectively, by $\Omega=\pi DdT$ and by $\Omega=Ad$, where d is the thickness of the BN sheet which is set to the interlayer distance of h-BN. D and T are the diameter and length of translational vector of the nanotube,[12] respectively. A is the area of the surface unit cell of the BN sheet. Furthermore, in the supercell approach to a single wire (an isolated slab), the periodic dipole images can give rise to a substantial depolarization field which not only affect the transverse component of the field-induced properties but also decrease rather slowly as the supercell dimension increases.[19] Therefore, the transverse dielectric constant, electric polarizability, and Born effective charges, presented below, have been corrected for this artificial depolarization field via one-dimensional Clausius-Mossotti relation[20] for the single BN sheet and two-dimensional Clausius-Mossotti relation[14,19] for the BN-NTs. We have checked numerically that the transverse component of these physical properties are independent of the supercell dimension used (within 1%) for the single BN sheet and also for the (5,0) BN-NT.

TABLE I. Lattice constants (a,c), static dielectric constant (ϵ), and Born effective charge (Z^*) of bulk BN in cubic, wurtzite, and hexagonal structures (denoted as c-BN, w-BN, and h-BN, respectively) as well as the isolated BN sheet. The available experimental values are listed in parentheses.

	c-BN	w-BN	h-BN	BN sheet
a	3.582 (3.615[a])	2.524 (2.558[a])	2.491 (2.50[b])	2.489
c	—	4.177 (4.228[a])	6.431 (6.65[b])	···
$\epsilon_\infty^{aa,bb}$	4.47 (4.5[c])	4.37 (4.95[d])	4.69	4.70
$\epsilon_{static}^{aa,bb}$	6.79 (7.1[c])	6.25 (6.85[d])	5.50	7.20, 5.80
ϵ_∞^{cc}		4.49 (4.10[d])	2.88	1.62
ϵ_{static}^{cc}		6.60 (5.06[d])	3.51	1.65
$Z^*_{a(b)}$	1.88 (1.98[e])	1.82	2.71	2.70
Z^*_c		1.91	0.86	0.25

[a]Taken from Ref. 21.
[b]Taken from Ref. 22.
[c]Taken from Ref. 23.
[d]Taken from Ref. 24.
[e]Taken from Ref. 25.

III. RESULTS AND DISCUSSION

A. Bulk BN structures and single BN sheet

The results for the bulk BN structures are summarized in Table I. All the theoretical lattice constants of all bulk BN structures agree rather well (within 1.5%) with the experimental values (see Table I), except c of h-BN which is 3.3% smaller than the experimental value. Interestingly, the static dielectric constants and Born effective charges of c-BN and w-BN are very similar, and the anisotropy for w-BN is rather small (Table I). This is due to the fact that although the layer stacking along the c direction of the wurtzite structure and the one along [111] direction of zinc-blende structure are different, the local tetrahedral atomic configuration is common to both structures. The calculated dielectric properties for c-BN and w-BN agree rather well (within 4.0%) with the available experimental values (see Table I). In contrast to w-BN, the anisotropy in the dielectric properties of h-BN is rather pronounced. For example, the Born effective charge for the field along the c axis (Z_c) is only about 1/3 of that for the field perpendicular to the c axis $[Z_{a(b)}]$ due to weak covalency along the c axis. Here **a** denotes one of the two in-plane primitive vectors [i.e., the vector connecting the two nearest neighboring B(N) atoms] and **b** is the vector that is perpendicular to **a**.

It is interesting to compare the last two columns (h-BN and BN sheet) in Table I. As h-BN is a one-dimensional stacking of BN sheets with rather large separation between neighboring sheets, it is natural to expect that both systems may have similar in-plane properties, as is actually seen in Table I except the static dielectric constant. While there is no in-plane anisotropy for the clamped-ion dielectric constant and Born effective charge for both h-BN and BN sheet, only

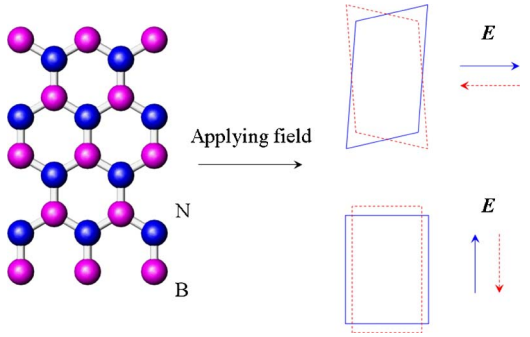

FIG. 1. (Color online) (a) Atomic arrangement of a single BN sheet and (b) schematic illustration of the mode of deformation of BN sheet under the in-plane electric field. Note that the magnitude of deformation is exaggerated.

the static dielectric constant of BN-NT shows strong in-plane anisotropy. The reason for this is that lattice strain is induced in a BN sheet under the in-plane electric field. The mode of strain is schematically shown in Fig. 1, where the magnitude of strain is much exaggerated. The strain mode is clearly anisotropic with respect to the direction of electric field and induces the anisotropy in the in-plane static dielectric constant for BN sheet. However, such a lattice strain cannot be induced in *h*-BN because of the alternating array of B and N along the *c* axis. The B and N arrangement of a given sheet is reversed in the neighboring sheets so that the strain induced by electric field in the neighboring BN sheets cancels out.

B. BN-NT

1. Longitudinal dielectric constant and electric polarizability

The calculated static electric polarizability α_{zz} and dielectric constant ϵ_{static} of the BN-NTs are plotted as a function of diameter (D) in Figs. 2 and 3, respectively. The electric polarizability of the BN-NTs is also listed in Table II. Figure 2(a) shows that on average, both the full (α_{zz}^{static}) and clamped-ion (electronic contribution only) (α_{zz}^{∞}) polarizabilities per unit length for the electric field parallel to the tube axis ($E\|\hat{z}$) are roughly proportional to the tube diameter, i.e., $\alpha=aD$, resembling the behavior of a thin dielectric cylindrical shell. This behavior is in strong contrast with the latest finding of $\alpha_{zz}\sim D^2+C$ for the CNTs from the density-functional perturbation theory (DFPT) calculations[19] and also with the recent finding from the IPLRT calculations.[11] Because the number of atoms on a BN-NT per unit length is proportional to D, this result indicates that every atom on the BN-NTs has nearly the same static polarizability, as would be the case for insulators. The slopes of α_{zz} are a_z=4.57 Å and $a_{z,0}$=3.08 Å for the full and clamped-ion polarizabilities, respectively. Note that the slope $a_{z,0}$ is nearly identical to the previous IPLRT calculations [3.04 Å,[12] 3.13 (Ref. 14)], indicating that local field effects for $E\|\hat{z}$ are indeed negligible. Indeed, the clamped-ion polarizabilities α_{zz}^{∞} listed in Table II are in good quantitative agreement with the corresponding values of $\alpha_{zz}(0)$ reported in Ref. 12. However, when the ionic contribution is included, as in the present calculations,

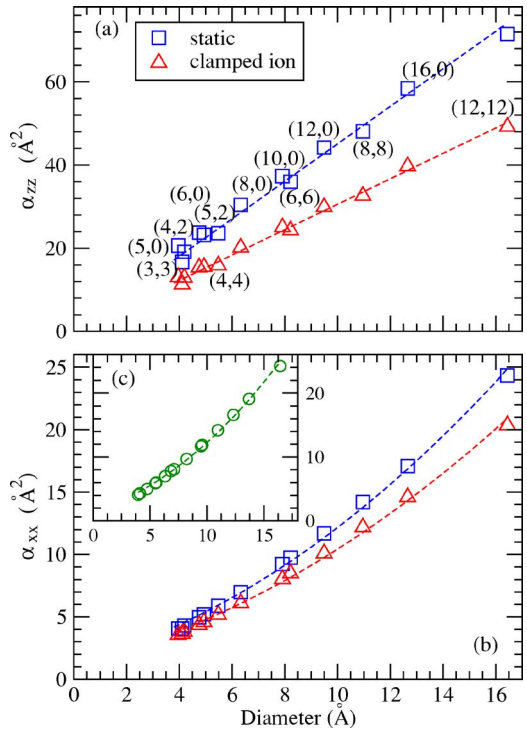

FIG. 2. (Color online) (a) Longitudinal (α_{zz}) and (b) [and inset (c)] transverse (α_{xx}) polarizabilities of BN-NTs as a function of the tube diameter (D). The plot in the inset (c) is generated by using the data from Table 1 in Ref. 26. The dashed lines in (a) are the straight lines fitted to the calculated polarizabilities (symbols), and in (b) and (c) are the function of $b(D+\delta)^2$ fitted to the calculated values.

the electric polarizability α_{zz} is significantly increased, by ~50%, demonstrating the importance of the ionic contribution. Very recently, *ab initio* calculations of the full and clamped-ion static electric polarizabilities of long BN-NTs within the framework of DFPT were reported.[26] It is gratifying that the α_{zz}^{static} and α_{zz}^{∞} listed in Table II agree very well with the corresponding longitudinal polarizabilities reported in Ref. 26. Furthermore, a linear line fitting to the longitudinal static polarizabilities listed in Table 1 in Ref. 26 gives

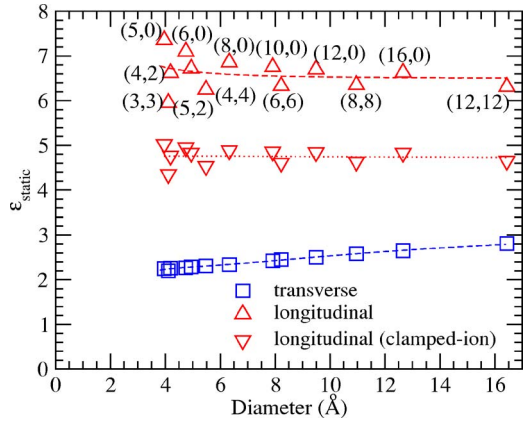

FIG. 3. (Color online) Full static dielectric constant of BN-NTs as a function of tube diameter. Each dashed line is the curve fitted to the corresponding calculated dataset. Longitudinal clamped-ion dielectric constants of BN-NTs are also plotted for comparison.

TABLE II. Full static (α^{static}) and clamped-ion (α^{∞}) electric polarizabilities and Born effective charge (Z^*) of the BN nanotubes.

Tube	$\alpha^{\infty}_{xx}, \alpha^{\infty}_{zz}$ (Å^2)	$\alpha^{static}_{xx}, \alpha^{static}_{zz}$ (Å^2)	Z^*_x, Z^*_y, Z^*_z (e)
(5,0)	3.56, 13.06	4.07, 20.64	0.34, 0.93, 2.87
(6,0)	4.36, 15.39	4.96, 23.76	0.32, 0.99, 2.83
(8,0)	6.11, 20.17	6.98, 30.43	0.30, 1.10, 2.78
(10,0)	8.04, 25.03	9.23, 37.33	0.29, 1.22, 2.75
(12,0)	10.10, 29.91	11.69, 44.20	0.28, 1.30, 2.74
(16,0)	14.61, 39.73	17.08, 58.43	0.27, 1.47, 2.72
(3,3)	3.64, 4.11	4.05, 16.69	0.37, 0.96, 2.56
(4,4)	5.19, 15.87	5.89, 23.59	0.33, 1.06, 2.62
(6,6)	8.49, 24.30	9.75, 35.96	0.29, 1.25, 2.66
(8,8)	12.18, 32.63	14.20, 48.09	0.28, 1.40, 2.67
(12,12)	20.36, 49.21	24.34, 71.52	0.27, 1.61, 2.69
(4,2)	3.81, 12.93	4.32, 19.14	0.36, 0.96, 2.65
(5,2)	4.59, 15.51	5.21, 23.17	0.33, 1.01, 2.70

rise to a slope of 4.58 Å, a value being almost identical to the slope (4.57 Å) reported above.

There is clear chirality dependence in α_{zz} and ϵ_{zz}, as shown in Figs. 2(a) and 3. We first discuss the clamped-ion dielectric constants, which are denoted by inverse triangles in Fig. 3 to simplify the problem. For a given diameter of BN-NT, zigzag BN-NTs have larger dielectric constant than armchair ones and the chiral ones are intermediate. The chirality dependence is strong for smaller diameters and tends to vanish as the diameter increases. The longitudinal dielectric constant of clamped-ion case clearly converges to 4.7 which is the clamped-ion dielectric constant of a single BN sheet, which is expected to be the case. The strong chirality dependence of clamped-ion longitudinal dielectric constant comes from the chirality dependence of the band gap. It was reported in Ref. 12 that the band gap of the zigzag BN-NTs would be reduced substantially as the tube diameter decreases, while that of the armchair BN-NTs depends on the diameter only slightly. It is known that the systems with a smaller band gap would have a larger dielectric constant. For static longitudinal dielectric constant, the present calculation takes account of only the relaxation of atomic positions with a fixed unit cell. Due to the difficulty in practical calculations, the shear deformation of the unit cell as observed in a single BN sheet (Fig. 1) is not taken into account. Therefore, the behavior of the static longitudinal dielectric constant shown by triangles in Fig. 2 is basically the same as those of clamped-ion case. The large diameter limit of static dielectric constant is about 6.4, which is close to the value for a single BN sheet obtained within the same constraint of atomic relaxation.

2. Transverse dielectric constant and electric polarizability

We begin our discussion with rather simple features. First, the transverse quantities [in Figs. 2(b) and 3] do not show appreciable chirality dependence for the whole range of diameter. Second, the ionic contribution is rather small, being only ~15% of the electronic contribution in the polarizability [Fig. 2(b)]. Third, the large diameter limit of transverse dielectric constant may be given by the circular average of the response of each part of the BN-NT surface, which may be approximated by $0.5(\epsilon^{aa,bb}_{static}+\epsilon^{c}_{static})$ with quantities for a single BN sheet. As we do not take account of the shear strain for BN-NT, $\epsilon^{aa,bb}_{static}$ is about 6.4 and the converged value of the squares (in Fig. 3) in the large diameter limit may be about 4.0.

The most surprising fact in the transverse quantities is that the transverse polarizability α_{xx} in Fig. 2(b) exhibits a rather different behavior.[12,14] In fact, $\alpha_{xx}(D)$ can be nicely fitted to $\alpha_{xx}=b(D+\delta)^2$, as can be seen from Fig. 2(b). This indicates that as far as the transverse dielectric properties are concerned, a BN-NT with a diameter, at least, up to ~15 Å studied here, behaves like a thin (nonideal) conducting cylindrical shell[27] (or a system of electrons moving freely on a cylindrical shell[13]) with an effective diameter of $D+\delta$. The parameters b and δ obtained by the fitting are, respectively, 0.0629 and 4.13 for the full polarizability, and 0.0523 and 4.40 for the clamped-ion polarizability. δ is slightly larger than the effective thickness ($d\sim 3.3$ Å) of the BN sheet mentioned above. The screening factor of the inner electric field (E_{in}) by a BN-NT is $E_{out}/E_{in}=1/(1-8b)\approx 2$ (E_{out} is the applied field outside the BN-NT) when the full response of the BN-NT is considered. Note that for a long classical dielectric cylindrical shell, the inner electric field $\mathbf{E}_{in}$ is also uniform and along $\mathbf{E}_{out}$. However, $E_{in}=4E_{out}\epsilon/[(\epsilon+1)^2-(\epsilon-1)^2(D+d)^2/(D-d)^2]$ would be enhanced rather than screened. For example, for the (8,8) BN-NT, the screening factor is 0.4 if ϵ^{xx}_{static} (2.58) [for the (8,8) BN-NT] is used or 0.8 if ϵ^{cc}_{static} (1.65) [for the BN sheet] is used. To see whether this phenomenological interpretation in terms of a thin conducting cylindrical shell is an accidental coincidence or not, we plot the calculated electric potential on a plane perpendicular to the tube axis of the (8,8) BN-NT in Fig. 4 (upper panel) and also calculate the total electric field along the applied electric field line going through the center of the BN-NT [Fig. 4 (lower panel)]. Figure 4 clearly shows that the electric field inside the BN-NT is indeed uniform and considerably reduced. The screening factor from Fig. 4 (lower panel) is 2.08 but not infinite, as would be expected from a perfect conducting cylindrical shell. We also plot the electric field for some other BN-NTs and find the same situation. Note that both the metallic and semiconducting CNTs exhibit the same behavior with a larger screening factor of 4.4.[19] Therefore, the transverse polarizability from the present finite-field calculations reveals a qualitatively different behavior, when compared with previous IPLRT calculations,[12,14] demonstrating the importance of taking the local field effects into account in this case. Again, the transverse polarizabilities listed in Table II are in good quantitative agreement with the corresponding values from the DFPT calculations very recently reported in Ref. 26. However, the calculated transverse polarizabilities were interpreted to be linearly related to the tube diameter in Ref. 26. Nevertheless, we plot the transverse static polarizability from Table 1 in Ref. 26 as a function of the tube diameter D, and find that it too can be nicely fitted by $\alpha_{xx}=b(D+\delta)^2$ with $b=0.0591$ and $\delta=4.53$ [see Fig. 2(c)].

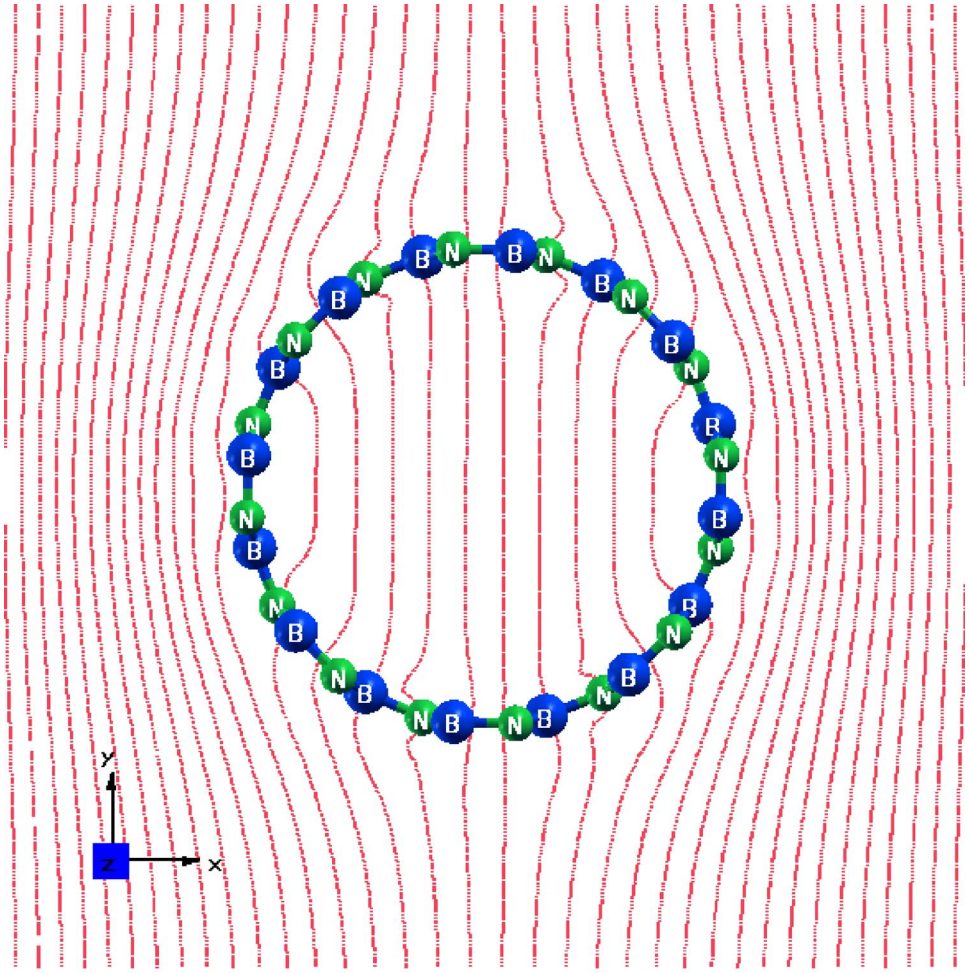

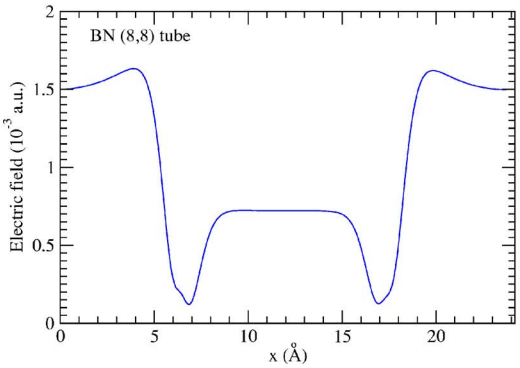

FIG. 4. (Color online) Upper panel: Potential contour plot on a *xy* plane perpendicular to the tube axis. Lower panel: The electric field along the line parallel to the *x* axis and going through the center of the BN-NT in the *xy* plane shown in the upper panel.

3. Born effective charges

To obtain the Born effective charges, we perform for each BN-NT three self-consistent finite-field calculations for the field applied along the three Cartesian coordinate axes, respectively. A Born effective charge tensor for each atom is then constructed from the field-induced atomic forces. These Born effective charge tensors are then diagonalized to give three principal components (Z_x^*, Z_y^*, Z_z^*). Interestingly, it turns out that Z_x^*, Z_y^* are for the transverse fields perpendicular to and tangential to the local tube surface of the ion concerned, respectively, while Z_z^* corresponds to the field along the tube axis. The calculated principal Born effective charges on all the BN-NTs studied here are displayed as a function of the tube diameter in Fig. 5.

Figure 5 shows that the medium component (Z_y^*) of the BN-NTs exhibits a pronounced monotonic dependence on the tube diameter (but independent of chirality), while the small component (Z_x^*) is almost a constant. In contrast, the large component (Z_z^*) shows a clear chirality-dependent oscillation superimposed on the mean value of 2.70*e* (the in-plane components of the Born effective charge of the single BN sheet) (see Fig. 5 and Table I). These interesting diameter dependence of Z_y^* and chirality dependence of Z_z^* suggest that one could determine both the diameter and chirality of a BN-NT by measuring its Born effective charges using, e.g., Raman and infrared spectroscopies. Characterization of the chirality and diameter of a BN-NT is still a great challenge.

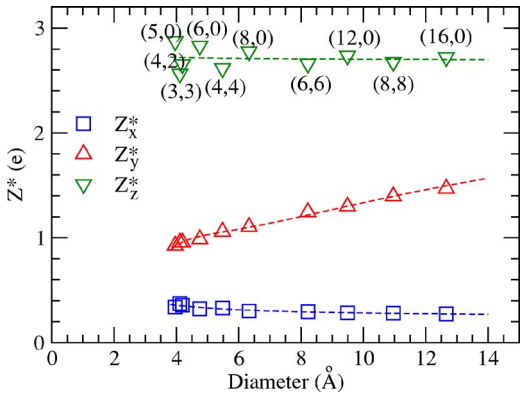

FIG. 5. (Color online) Three principal Born effective charges of BN-NTs as a function of tube diameter. Each dashed line is the curve fitted to the corresponding calculated dataset.

Interestingly, as the tube diameter becomes large, Z^*_x and Z^*_y tend to approach to the Z^*_c and $Z^*_{a(b)}$ components of the Born effective charge of the single BN sheet for the field perpendicular and parallel to the sheet plane (Table I), respectively. This is perhaps not surprising because the observed monotonic diameter dependence of the Z^*_x and Z^*_y merely reflects the degree of the local curvature of the BN-NTs with a finite diameter.

IV. CONCLUDING REMARKS

To summarize, we have carried out a systematic *ab initio* study of the static dielectric properties of the BN-NTs within density-functional theory with the LDA plus the latest finite-field electric-enthalpy theory. Specifically, the full static dielectric constant, electric polarizability, and Born effective charges of a number of BN-NTs, as well as the single graphitic BN sheet and bulk BN structures have been calculated. The calculated lattice constants, dielectric constants, and Born effective charges for the bulk BN structures are in good agreement with available experiments. We find that the ionic contribution to the static dielectric response of BN nanotubes (BN-NTs) is substantial and that a clear chirality-dependent oscillation is imposed on a linear relation between the longitudinal electric polarizability and the tube diameter, as for a thin dielectric cylindrical shell. We also find that the calculated features of the transverse dielectric response of the BN-NTs resemble that of a thin conducting cylindrical shell, with a screening factor of 2 for the inner electric field. Our calculations also show that for each BN-NT, the medium principal component of Born effective charge tensor has a pronounced dependence on diameter (but independent on chirality) and the large principal component exhibits a chirality dependence (but nearly independent on diameter), suggesting that a BN-NT could be characterized by measuring its Born effective charges using, e.g., Raman and infrared spectroscopies.

ACKNOWLEDGMENTS

We thank M. Kohyama and S. Tanaka for their help in developing the QMAS code. G.Y.G. gratefully acknowledges a guest researchership from the AIST of Japan. This work is partly supported by the Next Generation Supercomputing Project, Nanoscience Program and also partly by Grants-in-Aid for Scientific Research in Priority Area "Anomalous Quantum Materials," both from MEXT, Japan and also by the National Science Council, Ministry of Economic Affairs (93-EC-17-A-08-S1-0006) and NCTS of Taiwan.

*Electronic address: gyguo@phys.ntu.edu.tw

[1] S. Iijima, Nature (London) **354**, 56 (1991).
[2] S. J. Tans, A. R. M. Verschueren, and C. Dekker, Nature (London) **393**, 49 (1998).
[3] L. Liu, G. Y. Guo, C. S. Jayanthi, and S. Y. Wu, Phys. Rev. Lett. **88**, 217206 (2002).
[4] For example, N. G. Chopra, R. J. Luyken, K. Cherrey, V. H. Crespi, M. L. Cohen, S. G. Louie, and A. Zettl, Science **28**, 335 (1994); A. Loiseau, F. Willaime, N. Demoncy, G. Hug, and H. Pascard, Phys. Rev. Lett. **76**, 4737 (1996).
[5] X. Blase, A. Rubio, S. G. Louie, and M. L. Cohen, Europhys. Lett. **28**, 335 (1994).
[6] Y. Chen, J. Zou, S. J. Campbell, and G. L. Caer, Appl. Phys. Lett. **84**, 2430 (2004).
[7] Y. Zhang, A. Chang, J. Cao, Q. Wang, W. Kim, Y. Li, N. Morris, E. Yenilmez, J. Kong, and H. Dai, Appl. Phys. Lett. **79**, 3155 (2001); A. Ural, Y. Li, and H. Dai, *ibid.* **81**, 3464 (2002).
[8] J. Yu, Q. Zhang, J. Ahn, S. F. Yoon, Rusli, B. Gan, K. Chew, K. H. Tan, X. D. Bai, and E. G. Wang, J. Vac. Sci. Technol. B **19**, 671 (2001).
[9] R. Krupke, F. Hennrich, H. v. Loehneysen, and M. M. Kappes, Science **301**, 344 (2003); J. Li, Q. Zhang, N. Peng, and Q. Zhu, Appl. Phys. Lett. **86**, 153116 (2005).
[10] J. Kongsted, A. Osted, L. Jensen, P.-O. Astrand, and K. V. Mikkelsen, J. Phys. Chem. B **105**, 10243 (2001).
[11] G. Y. Guo, K. C. Chu, D.-S. Wang, and C.-G. Duan, Phys. Rev. B **69**, 205416 (2004); Comput. Mater. Sci. **30**, 269 (2004).
[12] G. Y. Guo and J. C. Lin, Phys. Rev. B **71**, 165402 (2005); **72**, 075416 (2005).
[13] L. X. Benedict, S. G. Louie, and M. L. Cohen, Phys. Rev. B **52**, 8541 (1995).
[14] L. Wirtz, M. Lazzeri, F. Mauri, and A. Rubio, Phys. Rev. B **71**, 241402(R) (2005).
[15] I. Souza, J. Iniguez, and D. Vanderbilt, Phys. Rev. Lett. **89**, 117602 (2002).
[16] P. Umari and A. Pasquarello, Phys. Rev. Lett. **89**, 157602 (2002).
[17] P. E. Blöchl, Phys. Rev. B **50**, 17953 (1994); G. Kresse and D. Joubert, *ibid.* **59**, 1758 (1999).
[18] S. Ishibashi, T. Tamura, S. Tanaka, M. Kohyama, and K. Terakura (unpublished).
[19] B. Kozinsky and N. Marzari, Phys. Rev. Lett. **96**, 166801 (2006).
[20] J. Tobik and A. Dal Corso, J. Chem. Phys. **120**, 9934 (2004).

[21] T. Soma, A. Sawaoka, and S. Saito, Mater. Res. Bull. **9**, 755 (1974).

[22] G. Cappellini, V. Fiorentini, K. Tenelsen, and F. Bechstedt, in *Gallium Nitride and Related Materials*, MRS Symposia Proceedings No. 395, edited by R. D. Dupuis, J. A. Edmond, F. A. Ponce, and S. Nakamura (Materials Research Society, Pittsburgh, 1996).

[23] P. J. Gielisse, S. S. Mitra, J. N. Plendl, R. D. Griffis, L. C. Mansur, R. Marshall, and E. A. Pascoe, Phys. Rev. **155**, 1039 (1967).

[24] R. Geick, C. H. Perry, and G. Rupprecht, Phys. Rev. **146**, 543 (1966).

[25] J. A. Sanjurjo, E. Lopez-Cruz, P. Vogl, and M. Cardona, Phys. Rev. B **28**, 4579 (1983).

[26] L. Wang, J. Lu, L. Lai, W. Song, M. Ni, Z. Gao, and W. N. Mei, J. Phys. Chem. C **111**, 3285 (2007).

[27] M. Krcmar, W. M. Saslow, and A. Zangwill, J. Appl. Phys. **93**, 3495 (2003).